Title

A Versatile In-Ear Biosensing System and Body-Area Network for Unobtrusive Continuous Health Monitoring.

Journal

IEEE Transactions on Biomedical Circuits and Systems, 17(3)

Authors

Paul, Akshay

Lee, Min

Xu, Yuchen

et al.

Publication Date

2023-06-01

DOI

10.1109/TBCAS.2023.3272649

Peer reviewed

HHS Public Access

Author manuscript

IEEE Trans Biomed Circuits Syst. Author manuscript; available in PMC 2024 July 12.

Published in final edited form as:

IEEE Trans Biomed Circuits Syst. 2023 June ; 17(3): 483–494. doi:10.1109/TBCAS.2023.3272649.

A Versatile In-Ear Biosensing System and Body-Area Network for Unobtrusive Continuous Health Monitoring

Akshay Paul [Student Member, IEEE],

Min S. Lee [Student Member, IEEE],

Yuchen Xu [Member, IEEE],

Stephen R. Deiss [Member, IEEE],

Gert Cauwenberghs [Fellow, IEEE]

Department of Bioengineering, University of California, San Diego, La Jolla, CA 92093 USA

Abstract

To enable continuous, mobile health monitoring, body-worn sensors need to offer comparable performance to clinical devices in a lightweight, unobtrusive package. This work presents a complete versatile wireless electrophysiology data acquisition system (weDAQ) that is demonstrated for in-ear electroencephalography (EEG) and other on-body electrophysiology with user-generic dry-contact electrodes made from standard printed circuit boards (PCBs). Each weDAQ device provides 16 recording channels, driven right leg (DRL), a 3-axis accelerometer, local data storage, and adaptable data transmission modes. The weDAQ wireless interface supports deployment of a body area network (BAN) capable of aggregating various biosignal streams over multiple worn devices simultaneously, on the 802.11n WiFi protocol. Each channel resolves biopotentials ranging over 5 orders of magnitude with a noise level of 0.52 μV_{rms} over a 1000-Hz bandwidth, and a peak SNDR of 119 dB and CMRR of 111 dB at 2 ksps. The device leverages in-band impedance scanning and an input multiplexer to dynamically select good skin contacting electrodes for reference and sensing channels. In-ear and forehead EEG measurements taken from subjects captured modulation of alpha brain activity, electroocoulogram (EOG) characteristic eye movements, and electromyogram (EMG) from jaw muscles. Simultaneous ECG and EMG measurements were demonstrated on multiple, freely-moving subjects in their natural office environment during periods of rest and exercise. The small footprint, performance, and configurability of the open-source weDAQ platform and scalable PCB electrodes presented, aim to provide the biosensing community greater experimental flexibility and lower the barrier to entry for new health monitoring research.

Keywords

BCI; in-ear EEG; health sensing; body sensor network; EOG; EMG; dry electrodes; PCB electrodes; WiFi

(Corresponding author: Akshay Paul.) A. Paul, a1paul@ucsd.edu; gert@ucsd.edu.

I. INTRODUCTION

BRAIN activity monitoring has significant implications for a variety of clinical and health applications, including disease diagnosis [1] and neurofeedback regulation [2]. Recent advancements in brain-computer interface (BCI) technology have enabled a broader range of everyday applications, such as motion control [3] and cognitive status monitoring [4], through the measurement of critical brain biomarkers. Noninvasive sensing using electroencephalography (EEG) continues to be a focus of study in order to increase the applicability and effectiveness of BCI in real-world applications. While full scalp cap systems and wet electrodes are still the de facto norm for EEG recordings, modern EEG systems incorporate dry contact electrodes and a reduced form factor to improve user comfort and wearability [5], [6]. Notable open-source efforts have put forward cost-effective acquisition platforms for scalp-based EEG brain monitoring [7], [8]. However, scalp-based EEG equipment still tends to be bulky and sensing from other locations on the body remains challenging as options for open-source wearable electrophysiology sensors is limited.

In-ear EEG originated as a novel sensing modality for capturing brain signals in a more comfortable, discrete, and unobtrusive manner from regions of the ear and ear canal [9], [10]. These in-ear systems can take various forms but in general have been comprised of custom-fitted earpieces embedded with dry-contact electrode materials with wired [11]–[13] and wireless [14]–[16] acquisition hardware, or as a generic fitting earpiece, with wired [17], [18] and wireless [19], [20] acquisition hardware. Only a limited number of in-ear systems however, have demonstrated a complete wearable earpiece with a wireless interface [21]–[23].

In-ear sensing is currently limited by electrode count, scalability of manufacturing, and intricate earpiece preparations [24]. A higher electrode count in each ear would offer potential benefits for motion artifact mitigation with independent component analysis techniques and a higher spatial resolution for mapping brain activity and electrodermal activity (EDA) across the ear canal [14], [25]–[27]. In-ear sensing has also been limited by the sampling rate available from wearable acquisition systems [28]. Certain electrophysiological experiments such as those involving fast event-related potentials (ERPs) [29], like the auditory brainstem response (ABR) [30], or biosignals with large bandwidths such as those found in electromyogram (EMG) [31], have not been demonstrated well from in-ear or wearable sensing systems, in part, because they necessitate a faster sampling rate (i.e. > 500 Hz) than those found conventionally in wearable recorders [32]. The utilization of in-ear sensing in mobile applications has been constrained by insufficient bandwidth of the wireless protocols implemented limiting measurement resolution. Expansion of in-ear sensing to accommodate additional sensing modalities and to enable incorporation into larger body-worn recording networks necessitates a high bandwidth wireless network. Despite recent efforts for around-the-ear sensing [33] and hearable platforms [34], open-source electrode designs and acquisitions hardware for in-ear monitoring still do not exist.

Therefore, the following aspects of a practical in-ear EEG system remain underdeveloped: (1) a low-cost, scalable onesize-fits-all earpiece with high density dry electrodes, (2) a

configurable, high-throughput acquisition system in a compact package, and (3) wireless transmission capability for untethered binaural measurement at high sampling rates.

The present study describes a wearable, wireless electrophysiology data acquisition system (weDAQ) with body-area network (BAN) capability (Fig. 1) and novel user-generic dry-contact electrodes (Fig. 2) that together, create a versatile, open-source platform for in-ear and on-body health sensing. Here we expand the hardware characterization and electrophysiology demonstration for this platform, originally introduced in [35]. To achieve low-cost, scalable electrodes, standard printed circuit board (PCB) manufacturing was utilized to produce a high electrode-count earpiece. The same process provides dry disk electrodes for surface measurement on the skin [36], [37]. To enable untethered monitoring, the weDAQ was designed with a high bandwidth wireless interface, small form factor, and configurable, low-noise ADCs to support fast sampling of multiple channels. Associated firmware for the system provides flexible configuration of multiple weDAQs on the BAN including transmission modes, dynamic rerouting of reference and driven-right-leg (DRL) active ground channels, and electrode-skin impedance monitoring. The electrodes were characterized using electrochemical impedance spectroscopy (EIS) and the wireless acquisition hardware was characterized for input-referred noise, data transmission reliability, and power consumption. Finally, a series of electrophysiological studies were conducted across multiple users including binaural in-ear and facial monitoring (Fig. 3) of eye blinks, alpha modulation, eye movements, and jaw muscle activity. An exercise electrophysiology study was also conducted capturing electrocardiogram and electromyogram from multiple subjects simultaneously. Performance of the platform is compared to state-of-the-art and commercial systems. In an effort to lower the barrier to entry for new research on in-ear sensing and wearable health monitoring, all hardware and software is provided as open-source (github.com/apaulworks) with compatibility to other open-source electrophysiology tools such as, OpenBCI, EEGLAB, and NeuroPype.

The paper is organized as follows: Section II further describes the user-generic in-ear and surface PCB electrodes, the weDAQ system, and the wireless body-area network. Section III provides the specifications for the electrophysiological experiments. Section IV presents hardware performance results for the weDAQ and the electrodes, and experimental results from the electrophysiology recordings. Section V provides a discussion for the design choices made and comparison of results from this work to the state-of-the-art. Section VI summarizes the work and lists the next steps for development.

II. HARDWARE IMPLEMENTATION

A. In-Ear and Surface Electrodes

The in-ear apparatus is comprised of 2 planar “crocodile” PCBs, mated together to form a 3D structure shown in Fig. 2(a,b). Each crocodile has 8 semi-circular silver (Ag) plated electrodes with a diameter of 2 mm and a 0.4 mm thickness. The jaws of the crocodile are made flexible because of the narrow design of the waist to fit snugly and comfortably inside the ear canal. Following mating, the 3D apparatus is connectorized with 30-AWG wire, coated with silver/silver chloride (Ag/AgCl) ink (Creative Materials, MA, USA), and cured at 80°C for 30 minutes (Fig. 2(c)). The coating can be made to extend over neighboring

semi-circular Ag contacts on each jaw of the crocodile to create larger effective electrodes, and a mask can be used for each Ag contact to form up to 16 individual electrodes. The Ag electrodes can also be bleached directly with oxidizing chlorine solution to form the AgCl layer, if ink is unavailable [38]. Surface disk electrodes had a diameter of 1 cm and were made using the same PCB process as the in-ear electrodes (Fig. 2(d)). Ag/AgCl ink was deposited onto the disk's Ag electrode contact and cured at 80°C for 60 minutes [38]. Again, 30 AWG wires were used for connectorizing and the back of the electrode was coated in polyimide (this gives the Ag electrode a yellow appearance) to insulate the connection (Fig. 2(e)). A clear, non-conductive lacquer or potting epoxy can be used to provide insulation and strain relief to the electrode-wire interface. Surface disk electrodes were attached to the skin using transparent double-sided medical tape (3M, MN, USA).

B. weDAQ System Overview

Sensors are interfaced to the weDAQ on a 18-pin locking zero insertion force (ZIF) connector compatible with standard flat flexible cable (FFC) ribbons (Fig. 1). To match the number of sensing channels available, 16 pins map to the inputs of the analog front-ends (AFE), 1 pin is a dedicated reference (SRB1), and the last pin is reserved as a dedicated body ground, (DRL). As shown in Fig. 4, each sensing path features a TVS diode array for ESD protection, a 2.2-kΩ resistor for patient protection, and a 1-nF capacitor for a low-pass filter with f_c = 72.5 kHz. The dedicated reference and DRL paths also have the patient protection resistor. The DRL features feedback circuit depicted in Fig. 5 is optimized for on-body electrophysiological sensing [27], where R_f is 1 MΩ and C_f is 1nF. The DRL electrode can be driven by a summing of the common-mode signals from any combination of channel AFEs on a single ADS1299 chip by configuring the *bias sensing* register or by both chips by closing the on-board switch between the 2 bias drive paths (Fig. 5).

The dedicated reference electrode can be disconnected from the SRB1 path by an on-board switch to allow for remapping of the reference to a different electrode from amongst those connected on the sensing input paths. This remapping of electrodes is accomplished by leveraging the highly configurable input MUX of the ADS1299 to switch any sensing electrode to a new reference using the SRB2 path in the event of poor contact or disconnection of the original dedicated reference, or for the case of measurement re-referencing. The same can be done for the remapping of the body ground from the dedicated DRL electrode to any of the available sensing electrodes using the BIASIN path, at the cost of giving up a sensing channel. The weDAQ system further utilizes the current sources and switches available on each channel of the ADS1299 to enable in-band electrode-skin impedance measurements before and after recordings, or out-of-band impedance scanning during sustained recordings. On-chip test signals and monitors can also be configured by software to calibrate and optimize the weDAQ for a given sensing application and user input.

The weDAQ device incorporates new and existing system designs [15], [27], [39] with commercial off-the-shelf (COTS) components in a small 3.5-cm x 4.0-cm 4-layer PCB centering around the ADS1299 bioinstrumentation IC [40] (Texas Instruments, TX, USA) (Fig. 6(a–c)). A 32-bit PIC microcontroller (MicroChip, AZ, USA) coordinates over an

SPI bus with 2 8-channel ADS1299 ICs, an ESP8266 WiFi module (Espressif, China), an accelerometer, and the SD flash memory (Fig. 6(b)). Power comes from a 3.7-V rechargeable LiPo battery which is regulated to produce a 3.3-V digital supply and the 2 analog supply rails, +2.5 V (AVDD) and −2.5 V (AVSS). The weDAQ can support up to a 2-kHz sampling rate across its 16 channels.

C. Body Area Network

The weDAQ devices use the 802.11n WiFi protocol to stream data. Firmware for the weDAQ system was implemented carefully on both the PIC mircocontroller and the ESP WiFi module to allow scalability of the BAN network (Fig. 6(e)), enhance reliability of the data recording, and optimize power consumption for a given application. The code base utilizes, in part, open source resources including OpenBCI and Brainflow. There are 3 main operating modes for weDAQ which are orchestrated by the custom firmware that include a half-duplex streaming mode (*HDX mode*), a unidirectional streaming mode (*simplex (SPX) mode*), and a non-transmit, local-write only mode (*dark mode*). The main advantages of the SPX mode are significant power savings by duty-cycling the WiFi modem and a decreased percentage of data drops at higher transmission rates. The SPX mode checks intermittently for new user configurations sent from a PC while providing continuous monitoring of the subject.

III. EXPERIMENTAL METHODS

A. Physiological Recording Configuration

Device configurations were sent over the air from a Python user interface to each weDAQ device. A referential (pseudomonopolar) montage was configured with a single reference shared by all 16 channels per board (Fig. 4). Gain was set to the maximum of 24 and common-mode bias sensing was performed on select channels before driving the dedicated DRL electrode (Fig. 5). Sampling was performed at 1 kHz and data was both streamed live over the WiFi connection through an access point (AP) to lab streaming layer (LSL) and saved locally on the SD card. Data streamed into LSL was processed, visualized, and saved in real-time on a laptop connected to the same AP. We utilized multiple weDAQ boards to support the binaural, facial, chest, and arm electrodes.

B. Electrode Placement

As mentioned above, electrodes were placed into each ear using 2 crocodile 3D in-ear devices. The 4 flanges of each in-ear device were oriented in superior (ExE), anterior (ExK), inferior (ExI), and posterior (ExP) directions. The flanges here serve to prevent the crocodile from ingressing too far into the ear canal but care should be taken when inserting anything into the ear canal. Optionally, as shown in Fig. 2(c), the 4 neighboring electrodes on each of the 4 jaws of the apparatus are shorted by the ink, creating a larger electrode surface area.

On the forehead, 6 dry contact disk electrodes were positioned in the F7, F8, Af7, Af8, Fp1, and Fp2 standard EEG locations (Fig. 3). An additional 2 disk electrodes were positioned under the left and right eye for EOG and 2 more disk electrodes were positioned on the left and right masseter jaw muscles [41]. Reference and DRL electrodes were placed on

the right mastoid bone behind the ear. Wire routing was managed behind the ear and along the temples with the same transparent double-sided medical tape used to mount the disk electrodes and weDAQ.

Subjects were fitted also with wet Ag/AgCl electrodes (3M RedDot) on the chest in the standard Lead II ECG configuration with the reference placed near the right collar bone, the sensing electrode at the bottom left edge of the ribcage, and the driven ground placed at the subject's left collar bone (Fig. 7). Another electrode was placed on either the right or left biceps, depending on the subject's preference. On the same arm, an additional weDAQ was mounted comfortably with an adjustable band to support the body measurements.

C. Experiment Protocol

Electrophysiological signals were recorded from 3 subjects using the weDAQ, crocodile in-ear PCB electrodes, and surface disk PCB electrodes, which included electroocoulogram (EOG), EMG, and EEG. For EOG, subjects were asked to blink at a 1 Hz metronome beat for 1 minute. Subsequently, EOG of eye movements was measured in 5 cycles, where the subjects directed their eye gaze from center to left then back to center, center to right then back to center, center to up then back to center, and center to down then back to center, taking 1 beat to move gaze and another to hold before the next movement. For EMG, jaw masseter muscle activity was measured during 10-second periods of clenching followed by 10 seconds of relaxing the jaw, for 2 cycles. Finally, for the EEG study, alpha band modulation was recorded with the subjects instructed to keep their eyes open and relaxed for a short period, followed by an eyes-closed period of 1 minute. The study was approved by the UC San Diego Institutional Review Board.

To further demonstrate the BAN, an exercise study was also performed with 2 independent, untethered subjects, each fitted with a weDAQ and electrodes on the chest and arm for mobile ECG and EMG (Fig. 7). First, a resting Lead II ECG was recorded as a baseline from both subjects simultaneously. Then, subjects were instructed to perform a short interval of a high-intensity exercise while their ECG was again recorded simultaneously. Muscle activity was tracked from the biceps while the subjects were instructed to lift, hold, and release a heavy object at timed intervals. Finally, EMG was monitored as the subjects rapidly lifted and released a heavy object to track burst muscle activity.

D. Data Analysis

Data was imported from LSL into EEGLAB [42] for analysis and bandpass filtered using channel-specific cutoff frequencies suitable for each electrophysiological modality. Spectrograms were generated for EOG channels during eye blinks and during jaw clenches from EMG channels. For eye movement analysis, in-ear channels were compared to forehead and facial EOG channels by measuring the voltage deflection seen at the onset and offset of the eye movement in the time series data; spectrograms were also generated for this comparison. Alpha modulation in the brain was compared using spectrograms taken from in-ear EEG channels and forehead EEG channels leading up to and during the onset of the eyes-closed task. To accommodate for channel offset and other variability, recordings from the 4 electrodes along each of the four flanges of the crocodile device were averaged.

IV. EXPERIMENTAL RESULTS

A. DAQ

In benchtop testing, the weDAQ performance was characterized across multiple sampling rates up to a maximum 4 kHz per channel. Input-referred noise (IRN) was measured with channels shorted to a reference DC voltage in a 10-second interval and with the electrodes connected (Fig. 8(a)). As expected for the configurable gain settings (i.e. 1, 2, 4, 6, 8, 12, and 24), IRN decreased with increasing gain across all tested sampling rates, and increased for a given gain setting as sampling rate increased (Fig. 9(a)). Over a 1000-Hz bandwidth (2 ksps) and gain 24, an IRN of 0.52 μV_{rms} and IRN density of 23 $nV/\sqrt{Hz}$ were measured. Signal-to-noise ratio (SNR) was calculated to be 98.1 dB at a sampling rate of 2 kHz and gain of 24 for a 10 Hz input test signal (Table I). Common-mode rejection ratio (CMRR) with a 60-Hz input signal was calculated to be 110.8 dB on average across channels and dynamic range (DR) was calculated to be 105.5 dB (Fig. 9(b)), for the same sampling rate and gain. A summary of weDAQ benchmark results are provided in Table I.

B. BAN

During testing of the BAN, we observed the WiFi network was able to support at least 4 weDAQ devices simultaneously streaming a total of 64 channels at 2 ksps. Reliability of the wireless stream was assessed using packet timestamps and parity checking to detect data drops or corruption. Fig. 9(c) shows the percentage of drops seen over a 1-hour period of streaming for the 3 transmission modes. During SPX streaming at 2 ksps, data drops averaged 0.005 %, and 0.75 % for HDX mode. In comparison, the dark mode which uses the wireless network only intermittently, experienced less than 0.0006 % data loss or corruption. The WiFi streaming bandwidth in close proximity to the access point (10 feet away) was confirmed to be 54 Mbps with the 4 streaming devices on the network.

Power consumption showed only a gradual increase with respect to sampling rate from 250 Hz to 4 kHz for all transmission modes (Fig. 9(d)). Each of the transmission modes showed a distinct separation in power usage across sampling frequencies. Specifically, at the 2-kHz sampling rate, HDX mode used the most power with 0.447 W (27.9 mW⁄ch), SPX mode in the middle with 0.224 W (14.0 mW/ch), and dark mode using the least with 0.171 W (10.7 mW⁄ch).

C. Electrodes

The user-generic dry PCB electrodes were performant to impedance, noise, and mechanical fit (i.e. remaining in good contact with the skin) criteria throughout the experiments for in-ear and forehead and facial placements. Electrochemical impedance spectroscopy (EIS) was performed on-body for these Ag/AgCl electrodes and compared to wet commercial Ag/AgCl electrodes (Fig. 8(b)). Results reveal DC impedance of 2.2 MΩ which linearly slopes downward from 2 MΩ at 10 Hz down to approximately 300 kΩ at 50 Hz. Phase for the ink electrodes starts close to 0° at DC compared to the commercial electrode at −30°. Both electrodes demonstrate a phase that decreases (become for negative) with respect to frequency, reaching approximately −60° and −80° at 500 Hz for ink and commercial, respectively.

EIS performed on ink electrodes after multiple days of electrophysiology experiments showed no significant change. Electrode performance for both in-ear and disk PCB electrodes remained consistent for the approximately 1-hour experiments performed on several days. Placement and alignment of the electrodes over the multiple days of experiments was aided by the use of fiducial markers on the subjects' skin to maintain comparable recording conditions between days and subjects. Some electrodes failed because of improper handling at the wire connection or at the ink's surface when storing the devices.

D. Eye Blinks and EMG

Eye blinks were detected from both in-ear and forehead channels, as well as, on the facial channels. Fig. 10(a) shows the recorded time series data and corresponding spectral signatures characteristic of eye blinks. Muscle activity from the jaw was detected robustly from the facial EMG electrodes, but was also picked up across some forehead and in-ear channels for intense muscle clenching events. Fig. 10(b) shows the corresponding time series data for the EMG activity shows strong electrical activity measured up to 1 mV and the characteristic spectral signature for intense muscle activity at 15 and 35 seconds and relaxed jaw from 0 to 15 and 25 to 35 seconds.

E. Alpha Power Modulation

Alpha modulation was observed well from both in-ear and forehead EEG electrodes. Fig. 11(a) shows the spectrogram for in-ear electrodes and Fig. 11(b) for the forehead electrodes during eyes open until 1 minute and eyes closed after. Power in the alpha band is observed to rise shortly after the subject closed their eyes at 1 minute. In-ear EEG and forehead EEG channels had on average equivalent power both before and after the 1 minute mark.

F. EOG of Eye Movement

Eye movements were also detected from in-ear and facial EOG channels with varying success. Specifically, facial EOG channels detected eye movements robustly seen as the blue and orange time traces in Fig. 12. Leftward eye movements created synchronous negative voltage deflection (Fig. 12(a)) and rightward created synchronous positive voltage deflections across both in-ear and facial disk electrodes (Fig. 12(b)). Upward eye movements created apposing deflections in the facial EOG electrodes (Fig. 12(c)) and the opposite apposing deflection was seen for downward eye movement (Fig. 12(d)), as expected. However, upward and downward eye movements were not detected well from in-ear channels (Fig. 12(c,d)).

G. Multi-Subject Exercise

During exercise monitoring, the weDAQ BAN clearly captured ECG and EMG signals from the subjects simultaneously throughout the study. In Fig. 13(a), the resting ECG waveform shows a distinct difference in resting heart rate between the 2 subjects. Subject 1, in black, had a R-R interval of 1.10 s for a resting heart rate of 54.5 bpm compared to Subject 2, in blue, with a R-R interval of 0.83 s for a resting heart rate of 72.3 bpm. During exercise, Subject 1 presented a heart rate 108 bpm and Subject 2 presented a 96 bpm heart rate. The P-QRS-T signatures were clearly presented and differentiable from the live ECG data

stream. In Fig. 13(b), during sustained lift-and-hold activity, Subjects 1 and 2 both presented clear muscle activity seen in the EMG recording. In the burst lift-and-release activity, Subject 2 muscle activity was clearly detected and smaller in duration and amplitude than their lift-and-hold EMG recording. Subject 1 reported to having to use less muscle power to lift and release the object than during the hold activity, which could explain the diminished EMG activity seen here.

V. DISCUSSION

The weDAQ demonstrated performance results comparable to current custom or commercially available electrophysiology recording systems (Table II), with advantages in sampling rate, input range, measurement bandwidth, and wireless transmission bandwidth. The weDAQ does however consume more power primarily because of the WiFi module but still offers all-day wearability with small LiPo batteries and power-saving transmission modes. Specifically, the SPX streaming mode provided a balance of high sampling rate with minimal streaming data loss and greater energy efficiency compared to normal HDX streaming thanks to duty cycling of the wireless transmission. The dry PCB electrodes presented were reliable over several days, maintaining phase integrity and a 50 Hz impedance of approximately 1 MΩ. The crocodiles outperformed comparable devices (Table III) in electrode count and fabrication scalability. In-ear crocodile electrodes performed well in the electrophysiology testing compared to the dry disk electrodes placed on the forehead and face. The crocodile electrodes connected with the weDAQ captured eye blinks, jaw EMG activity, and alpha power modulation in the brain. For detection of eye movements however, electrophysiological signals captured from in-ear channels were considerably less conclusive than facial and forehead place EOG channels but blinks were still well captured. Although sometimes considered an artifact in EEG measurements, the detection of eye blinks can serve as a reliable marker for sleep staging and validation of the sensing system while streaming [45], [46]. The deployment of multiple streaming weDAQ devices on the BAN was further demonstrated for monitoring multiple subjects during the exercise physiology experiment in which Lead II ECG and biceps EMG activity were well captured.

WiFi was chosen because it supports up to 25x the transmission bandwidth of Bluetooth and is more amenable to forming the BAN. Operating on the 802.11 protocol allows use in nearly all settings and modification of the firmware by the end users. Whereas devices operating on the 802.15 medical body-area network (MBAN) are restricted to usage in only healthcare facilities and must register for approval. We were also able to implement different modes of transmission by leveraging in-house and open-source firmware resources for WiFi to save power and better suit the application-specific needs of in-ear sensing or on-body health monitoring.

In terms of general usability of the weDAQ, we found the device to be plug-and-play in most cases. Connection to the WiFi network on device start-up and data streaming can be affected by other traffic on the network but simple fixes have been to use a dedicated access point on a channel with less traffic. Using 3D printed enclosures, the weDAQ can be easily mounted to almost any part of the body with either a clip, strap, or adhesive tape (Fig. 6(f)). In-ear electrodes were easy to assemble and worked reliably for the duration of the study and were

even seen to work after several months of storage. Crocodile devices fit snugly into the ears of subjects tested and remained electrodes remained mechanically stable. In some cases of subjects sweating or moving vigorously, the electrodes were observed slipping out of the ear canal but generally stayed in place.

Finally, we chose to make the weDAQ and PCB electrodes out of COTS components and provide all associated designs open-source to the community as a high-performance tool kit to lower the barrier of entry into niche research areas like in-ear EEG. End users can further enhance the versatility of this sensing platform by tuning the hardware, software, and firmware to fit their specific needs. The weDAQ and accompanying electrodes are well suited to conduct electrophysiological studies involving multiple subjects and/or the need for subjects to move around. For example, studies involving students in classrooms that seek to monitor neural markers for cognitive engagement and social behavior under naturalistic conditions [47], [48], or studies seeking to monitor brain dynamics and motion artifacts during walking [49] or while using multi-modal sensors to track drivers and passengers in a car [50], would benefit from BANs with wearable recording units.

VI. CONCLUSION

We presented a low-profile user-generic and portable ExG instrumentation device with versatile capabilities for in-ear and on-body biosensing. The electrodes were easy to make and reliable for measurements of in-ear and forehead EEG, EOG, and EMG. The weDAQ system captured biosignals from multiple subjects at a high sampling rate and data quality comparable to clinical systems, including in-ear EEG signals during an alpha modulation task, eye blinks, and eye movements. Facial electrodes further captured eye movements and muscle activity from the jaw. Electrode sensors and weDAQ devices were also demonstrated for multi-subject recording during physical activity. The weDAQ creates a body area network to reliably capture and stream electrophysiological data. The custom scalable firmware and high degree of input configurability have enabled this platform to perform well in each of these applications. The next steps for weDAQ development include improving energy efficiency, demonstrating the input MUX for dynamic rerouting of reference and DRL, and utilizing out-of-band frequencies for continuous electrode-skin impedance monitoring. For the in-ear electrodes, improvements can be made to include integrated reference and DRL electrodes and to implement a standard connector interface. This work paves the way for high-channel count, fast sampling body area networks for mobile health sensing and intelligent closed-loop brain computer interfaces.

ACKNOWLEDGMENT

The authors thank W. David Hairston, PhD and Michael Nonte from the Army Research Lab for helpful technical discussions. The authors thank the open-source electrophysiology community and forums.

This work was supported in part by the University of California San Diego Center for Wearable Sensors.

REFERENCES

[1]. Rodrigues PM, Bispo BC, Garrett C, Alves D, Teixeira JP, and Freitas D, “Lacsogram: A new EEG tool to diagnose alzheimer’s disease,” IEEE Journal of Biomedical and Health Informatics, vol. 25, no. 9, pp. 3384–3395, 2021. [PubMed: 33784628]

[2]. Pei G, Guo G, Chen D, Yang R, Shi Z, Wang S, Zhang J, and Wu J, “BrainKilter: A real-time EEG analysis platform for neurofeedback design and training,” IEEE Access, vol. 8, p. 13, 2020.

[3]. An H-S, Kim J-W, and Lee S-W, “Design of an asynchronous brain-computer interface for control of a virtual avatar,” 2016 4th International Winter Conference on Brain-Computer Interface (BCI), pp. 1–2, 2016.

[4]. Kim D, Park J, Hwang J, Cho WH, and Lee SW, “Decoding prefrontal cognitive states from electroencephalography in virtual-reality environment,” 2020 8th International Winter Conference on Brain-Computer Interface (BCI), pp. 1–3, 2020.

[5]. Huang Y-J, Wu C-Y, Wong AM-K, and Lin B-S, “Novel active comb-shaped dry electrode for EEG measurement in hairy site,” IEEE Transactions on Biomedical Engineering, vol. 62, no. 1, pp. 256–263, 2015. [PubMed: 25137719]

[6]. O’Sullivan M, Pena JP, Bocchino A, O’Mahony C, Costello D, Popovici E, and Temko A, “Comparison of electrode technologies for dry and portable EEG acquisition,” 2017 7th IEEE International Workshop on Advances in Sensors and Interfaces (IWASI), pp. 15–20, 2017.

[7]. OpenBCI, “Cyton board 8-channels,” https://docs.openbci.com/.

[8]. Teversham J, Wong SS, Hsieh B, Rapeaux A, Troiani F, Savolainen O, Zhang Z, Maslik M, and Constandinou TG, “Development of an ultra low-cost SSVEP-based BCI device for real-time on-device decoding,” in 2022 44th Annual International Conference of the IEEE Engineering in Medicine & Biology Society (EMBC), pp. 208–213, 2022.

[9]. Looney D, Kidmose P, Park C, Ungstrup M, Rank ML, Rosenkranz K, and Mandic DP, “The in-the-ear recording concept:User-centered and wearable brain monitoring,” IEEE Pulse, vol. 3, no. 6, pp. 32–42, 2012. [PubMed: 23247157]

[10]. Goverdovsky V, Looney D, Kidmose P, and Mandic DP, “In-ear EEG from viscoelastic generic earpieces: Robust and unobtrusive 24/7 monitoring,” IEEE Sensors Journal, vol. 16, no. 1, pp. 271–277, 2016.

[11]. Looney D, Park C, Kidmose P, Rank ML, Ungstrup M, Rosenkranz, and Mandic DP, “An in-the-ear platform for recordingelectroencephalogram,” in 2011 Annual International Conference of the IEEE Engineering in Medicine and Biology Society, pp. 6882–6885, 2011.

[12]. Kidmose P, Looney D, Ungstrup M, Rank ML, and Mandic DP, “A study of evoked potentials from ear-EEG,” IEEE Transactions on Biomedical Engineering, vol. 60, no. 10, pp. 2824–2830, 2013. [PubMed: 23722447]

[13]. Zhou X, Li Q, Kilsgaard S, Moradi F, Kappel SL, and Kidmose P, “A wearable ear-EEG recording system based on dry-contact active electrodes,” in 2016 IEEE Symposium on VLSI Circuits, pp. 1–2, IEEE, 2016.

[14]. Kappel SL, Rank ML, Toft HO, Andersen M, and Kidmose P, “Dry-contact electrode ear-EEG,” IEEE Transactions on Biomedical Engineering, vol. 66, no. 1, pp. 150–158, 2019. [PubMed: 29993415]

[15]. Paul A, Akinin A, Lee MS, Kleffner M, Deiss SR, and Cauwenberghs G, “Integrated in-ear device for auditory health assessment,” in 2019 41st Annual International Conference of the IEEE Engineering in Medicine and Biology Society (EMBC), pp. 56–59, 2019.

[16]. Jeong D-H and Jeong J, “In-ear EEG based attention state classification using echo state network,” Brain Sciences, vol. 10, p. 321, May 2020. [PubMed: 32466505]

[17]. Bertelsen AR, Bladt H, Christensen CB, Kappel SL, Toft HO, Rank ML, Mikkelsen KB, and Kidmose P, “Generic dry-contact ear-EEG,” in 2019 41st Annual International Conference of the IEEE Engineering in Medicine and Biology Society (EMBC), pp. 5552–5555, 2019.

[18]. Tabar YR, Mikkelsen KB, Shenton N, Kappel SL, Bertelsen AR, Nikbakht R, Toft HO, Henriksen CH, Hemmsen MC, Rank ML, Otto M, and Kidmose P, “At-home sleep monitoring using generic ear-EEG,” Frontiers in Neuroscience, vol. 17, p. 987578, Feb. 2023.

[19]. Mikkelsen KB, Kappel SL, Mandic DP, and Kidmose P, “EEG recorded from the ear: Characterizing the ear-EEG method,” Frontiers in Neuroscience, vol. 9, p. 438, 2015. [PubMed: 26635514]

[20]. Goverdovsky V, von Rosenberg W, Nakamura T, Looney D, Sharp DJ, Papavassiliou C, Morrell MJ, and Mandic DP, “Hearables: Multimodal physiological in-ear sensing,” Scientific Reports, vol. 7, no. 1, 2017.

[21]. Lee J, Lee K-R, Ha U, Kim J-H, Lee K, Gweon S, Jang J, and Yoo H-J, “A 0.8-V 82.9-μW in-ear BCI controller IC with 8.8 PEF EEG instrumentation amplifier and wireless BAN transceiver,” IEEE Journal of Solid-State Circuits, vol. 54, no. 4, pp. 1185–1195, 2019.

[22]. Kaveh R, Doong J, Zhou A, Schwendeman C, Gopalan K, Burghardt FL, Arias AC, Maharbiz MM, and Muller R, “Wireless user-generic ear EEG,” IEEE Transactions on Biomedical Circuits and Systems, vol. 20, no. 4, pp. 727–737, 2020.

[23]. Schwendeman C, Kaveh R, and Muller R, “Drowsiness detection with wireless, user-generic, dry electrode ear EEG,” in 2022 44th Annual International Conference of the IEEE Engineering in Medicine and Biology Society (EMBC), pp. 9–12, 2022.

[24]. Röddiger T, Clarke C, Breitling P, Schneegans T, Zhao H, Gellersen H, and Beigl M, “Sensing with earables: A systematic literature review and taxonomy of phenomena,” Proceedings of the ACM on Interactive, Mobile, Wearable and Ubiquitous Technologies, vol. 6, no. 3, pp. 1–57, 2022.

[25]. Makeig S, “Independent component analysis of EEG data,” Advances in Neural Information Processing Systems (NIPS), 1995.

[26]. Makeig S, “Evaluation of artifact subspace reconstruction for automatic artifact components removal in multi-channel EEG recordings,” IEEE Transactions on Biomedical Engineering, 2019.

[27]. Paul A, Deiss SR, Tourtelotte D, Kleffner M, Zhang T, and Cauwenberghs G, “Electrode-skin impedance characterization of in-ear electrophysiology accounting for cerumen and electrodermal response,” in IEEE Neural Engineering (NER), pp. 855–858, IEEE, 2019.

[28]. Ne CKH, Muzaffar J, Amlani A, and Bance M, “Hearables, in-ear sensing devices for bio-signal acquisition: A narrative review,” Expert Review of Medical Devices, vol. 18, no. sup1, pp. 95–128, 2021. [PubMed: 34904507]

[29]. Picton TW, Lins OG, and Scherg M, “The recording and analysis of event-related potentials,” Handbook of neuropsychology, vol. 10, pp. 3–3, 1995.

[30]. Boston JR, “Spectra of auditory brainstem responses and spontaneous EEG,” IEEE Transactions on Biomedical Engineering, no. 4, pp. 334–341, 1981. [PubMed: 7287033]

[31]. Merletti R and Farina D, Surface electromyography: Physiology, engineering, and applications. John Wiley & Sons, 2016.

[32]. Akinin A, Paul A, Wang J, Buccino A, and Cauwenberghs G, “Biopotential measurements and electrodes,” in Neural Engineering, pp. 65–96, Springer, Cham, 2020.

[33]. Knierim MT, Berger C, and Reali P, “Open-source concealed EEG data collection for Brain-computer-interfaces - neural observation through OpenBCI amplifiers with around-the-ear cEEGrid electrodes,” Brain-Computer Interfaces, vol. 8, pp. 161–179, Oct. 2021.

[34]. Röddiger T, King T, Roodt DR, Clarke C, and Beigl M, “OpenEarable: Open hardware earable sensing platform,” in Proceedings of the 1st International Workshop on Earable Computing, EarComp, vol. 22, pp. 29–34, 2022.

[35]. Paul A, Lee M, Xu Y, Deiss S, and Cauwenberghs G, “A versatile in-ear biosensing system for continuous brain and health monitoring,” in 2022 IEEE International Symposium on Circuits and Systems (ISCAS), pp. 620–624, 2022.

[36]. Chi YM, Jung T-P, and Cauwenberghs G, “Dry-contact and noncontact biopotential electrodes: Methodological review,” IEEE Reviews in Biomedical Engineering, vol. 3, pp. 106–119, 2010. [PubMed: 22275204]

[37]. Chi YM, Wang Y-T, Wang Y, Maier C, Jung T-P, and Cauwenberghs G, “Dry and noncontact EEG sensors for mobile brain–computer interfaces,” IEEE Transactions on Neural Systems and Rehabilitation Engineering, vol. 20, no. 2, pp. 228–235, 2012. [PubMed: 22180514]

[38]. Lee MS, Paul A, Xu Y, Hairston WD, and Cauwenberghs G, “Characterization of Ag/AgCl electrode fabrication methods,” Frontiers in Electronics, 2021.

[39]. Samson VRR, “Electroencephalogram-based OpenBCI devices for disabled people,” Proc. Conf. Micro-Electronics, 2018.

[40]. Rashid U, Niazi I, Signal N, and Taylor D, “An EEG experimental study evaluating the performance of Texas Instruments ADS1299,” Sensors, vol. 18, p. 3721, Nov. 2018. [PubMed: 30388836]

[41]. Prum G, Ten Bosch J, and de Jongh H, “Jaw muscle EMG-activity and static loading of the mandible,” Journal of Biomechanics, 1978.

[42]. Delorme A and Makeig S, “EEGLAB: an open-source toolbox for analysis of single-trial EEG dynamics,” Journal of Neuroscience Methods, 2004.

[43]. Tang T, Yan L, Park JH, Wu H, Zhang L, Lee HYB, and Yoo J, “34.6 EEG dust: A BCC-based wireless concurrent recording/transmitting concentric electrode,” in 2020 IEEE International SolidState Circuits Conference - (ISSCC), pp. 516–518, 2020.

[44]. Siddharth, Patel AN, Jung T-P, and Sejnowski TJ, “A wearable multi-modal bio-sensing system towards real-world applications,” IEEE Transactions on Biomedical Engineering, vol. 66, no. 4, pp. 1137–1147, 2019. [PubMed: 30188809]

[45]. Pham N, Dinh T, Kim T, Raghebi Z, Bui N, Truong H, Nguyen T, Banaei-Kashani F, Halbower A, Dinh T, Nguyen P, and Vu T, “Detection of microsleep events with a behind-the-ear wearable system,” IEEE Transactions on Mobile Computing, vol. 22, pp. 841–857, Feb. 2023.

[46]. Chi Y and Cauwenberghs G, “Micropower non-contact EEG electrode with active common-mode noise suppression and input capacitance cancellation,” in 2009 Annual International Conference of the IEEE Engineering in Medicine and Biology Society, (Minneapolis, MN), pp. 4218–4221, IEEE, Sept. 2009.

[47]. Dikker S, Wan L, Davidesco I, Kaggen L, Oostrik M, McClintock J, Rowland J, Michalareas G, Van Bavel JJ, Ding M, and Poeppel D, “Brain-to-brain synchrony tracks real-world dynamic group interactions in the classroom,” Current biology, vol. 27, no. 9, pp. 1375–1380, 2017. [PubMed: 28457867]

[48]. Poulsen AT, Kamronn S, Dmochowski J, Parra LC, and Hansen LK, “EEG in the classroom: Synchronised neural recordings during video presentation,” Scientific reports, vol. 7, no. 1, pp. 1–9, 2017. [PubMed: 28127051]

[49]. Nordin AD, Hairston WD, and Ferris DP, “Faster gait speeds reduce alpha and beta EEG spectral power from human sensorimotor cortex,” IEEE Transactions on Biomedical Engineering, vol. 67, no. 3, pp. 842–853, 2019. [PubMed: 31199248]

[50]. Biswas S, Chambers D, Hairston WD, and Bhattacharya S, “Head pose classification for passenger with CNN,” Transportation Engineering, p. 100157, 2022.

[51]. Hölle D, Meekes J, and Bleichner MG, “Mobile ear-EEG to study auditory attention in everyday life,” Behavior research methods, vol. 53, no. 5, pp. 2025–2036, 2021. [PubMed: 33721208]

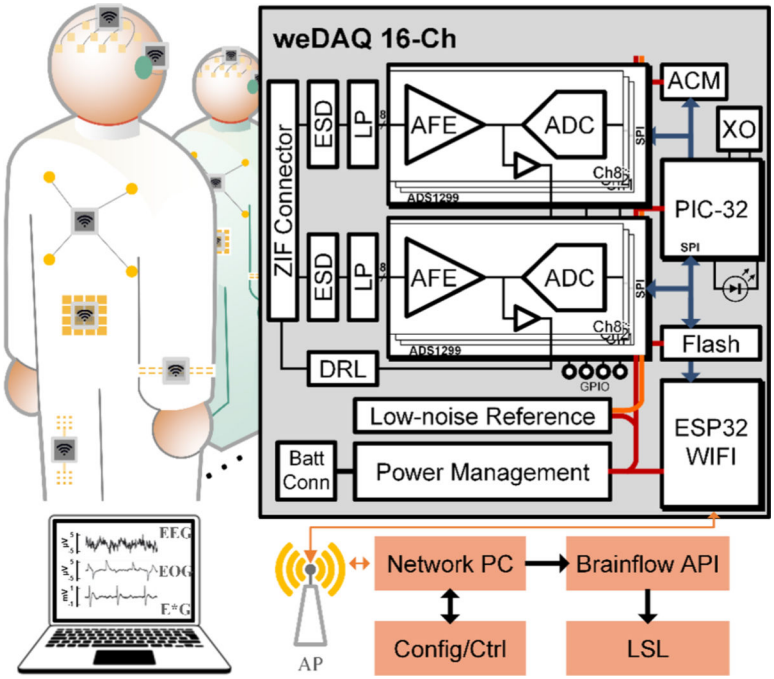

Fig. 1.

Wireless electrophysiology data acquisition (weDAQ) in the setting of a body-sensor network where multiple devices are deployed onto a subject or cohort of subjects.

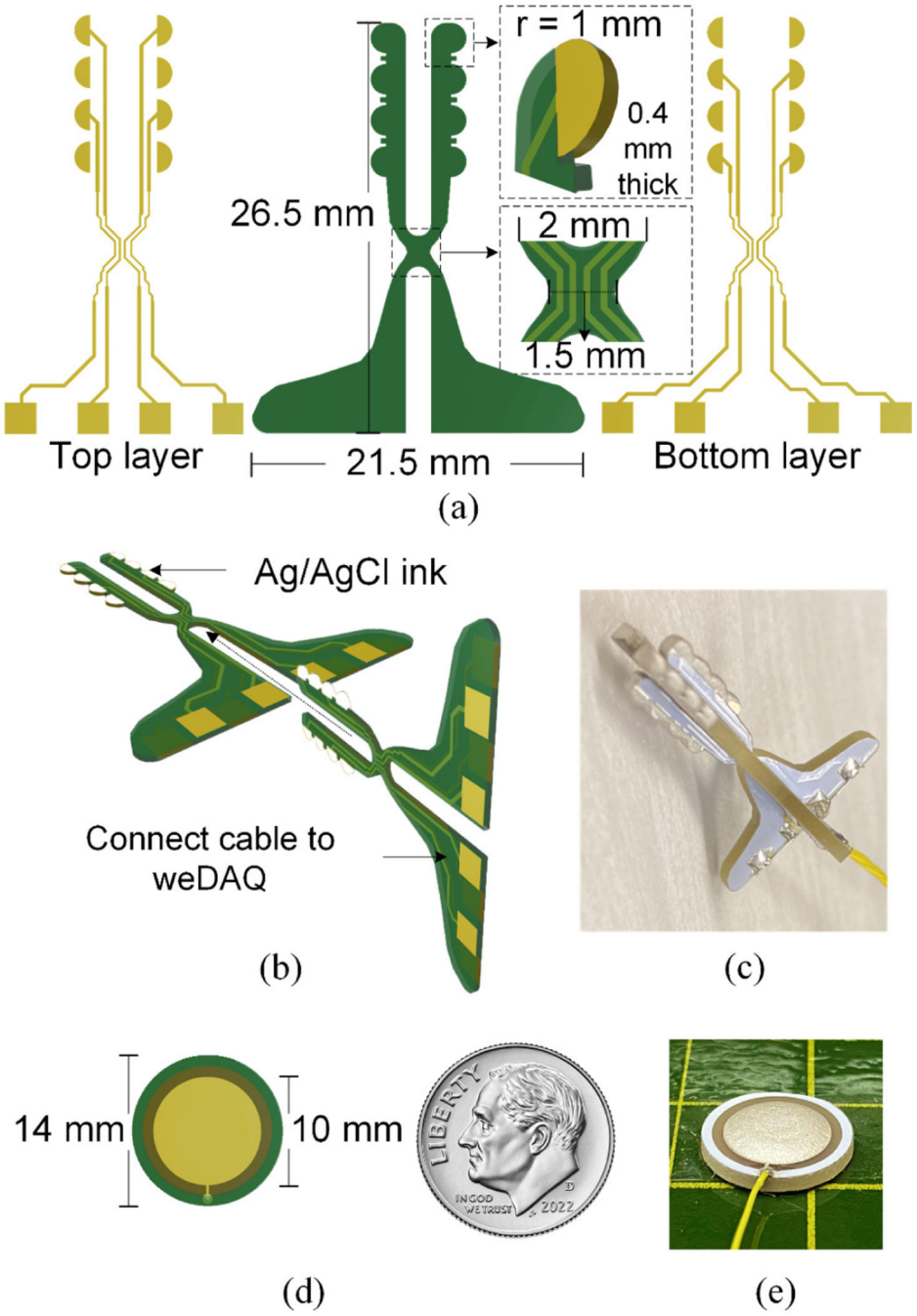

Fig. 2.

(a) Copper metal layers and overall dimensions of the “crocodile” PCB in-ear electrode. (b) Assembly of 2 8-electrode crocodiles into a single, 16-electrode 3D in-ear apparatus with 4 flanges. (c) Fully assembled crocodile with Ag plated electrodes coated with a cured layer of Ag/AgCl ink. (d) Flat disk PCB electrode for general body area sensing, (e) with wired connection and Ag/AgCl ink cured onto Ag plated top metal.

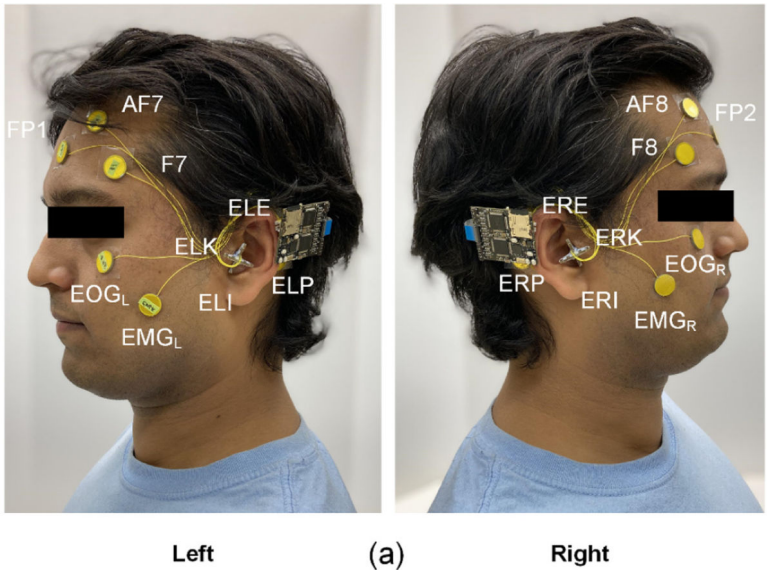

Fig. 3.

An untethered subject wearing in-ear crocodile and surface disk electrodes supported by 2 weDAQs.

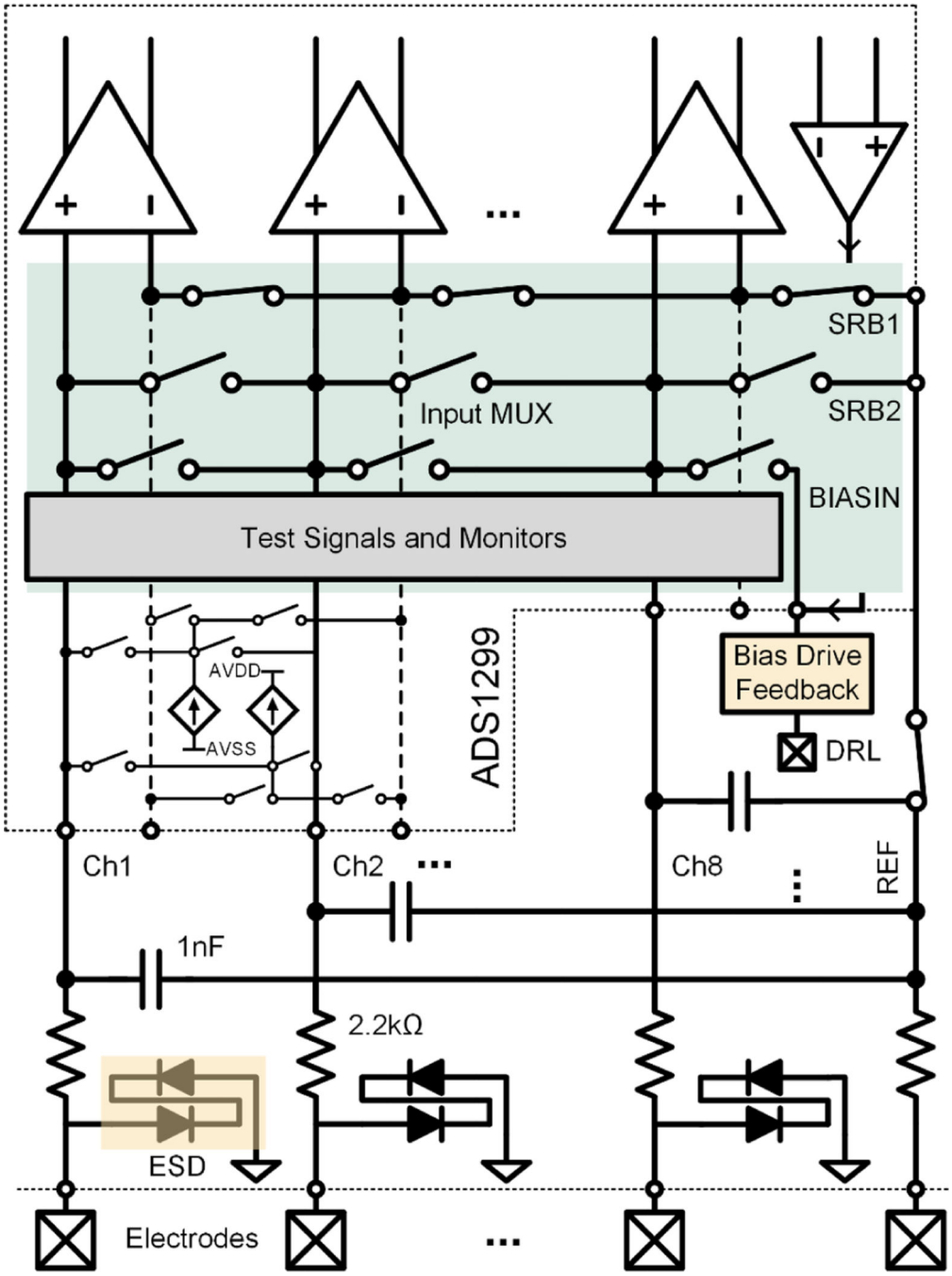

Fig. 4.

Analog front-end of the weDAQ accommodating a variety of electrophysiological signals using both dry and wet electrodes, incorporating electrostatic discharge (ESD) protection, patient-protection resistors, and a low-pass filter. The weDAQ firmware takes full advantage of the ADS1299 input mux for rerouting of reference and driven-right-leg paths from their default paths (SRB1) and (DRL), respectively, to any electrode via the SRB2 and BIASIN paths. In addition, the front-end supports impedance scanning to verify electrode contact quality and detect electrodermal physiological activity.

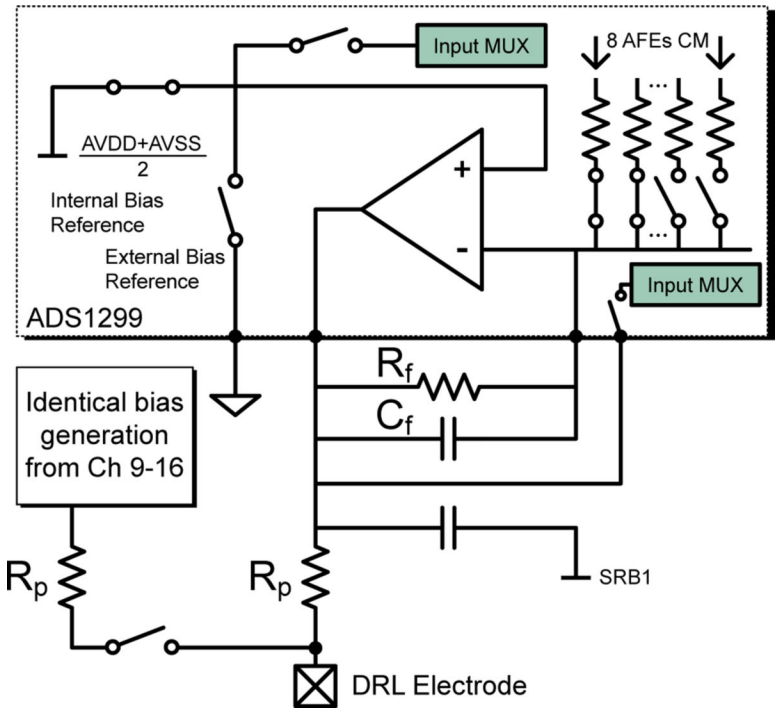

Fig. 5.

Diagram of the driven right leg (bias drive) circuit. The DRL electrode contacting the body is driven by either an internal or externally provided reference voltage and by the common-mode signals from select channel amplifiers.

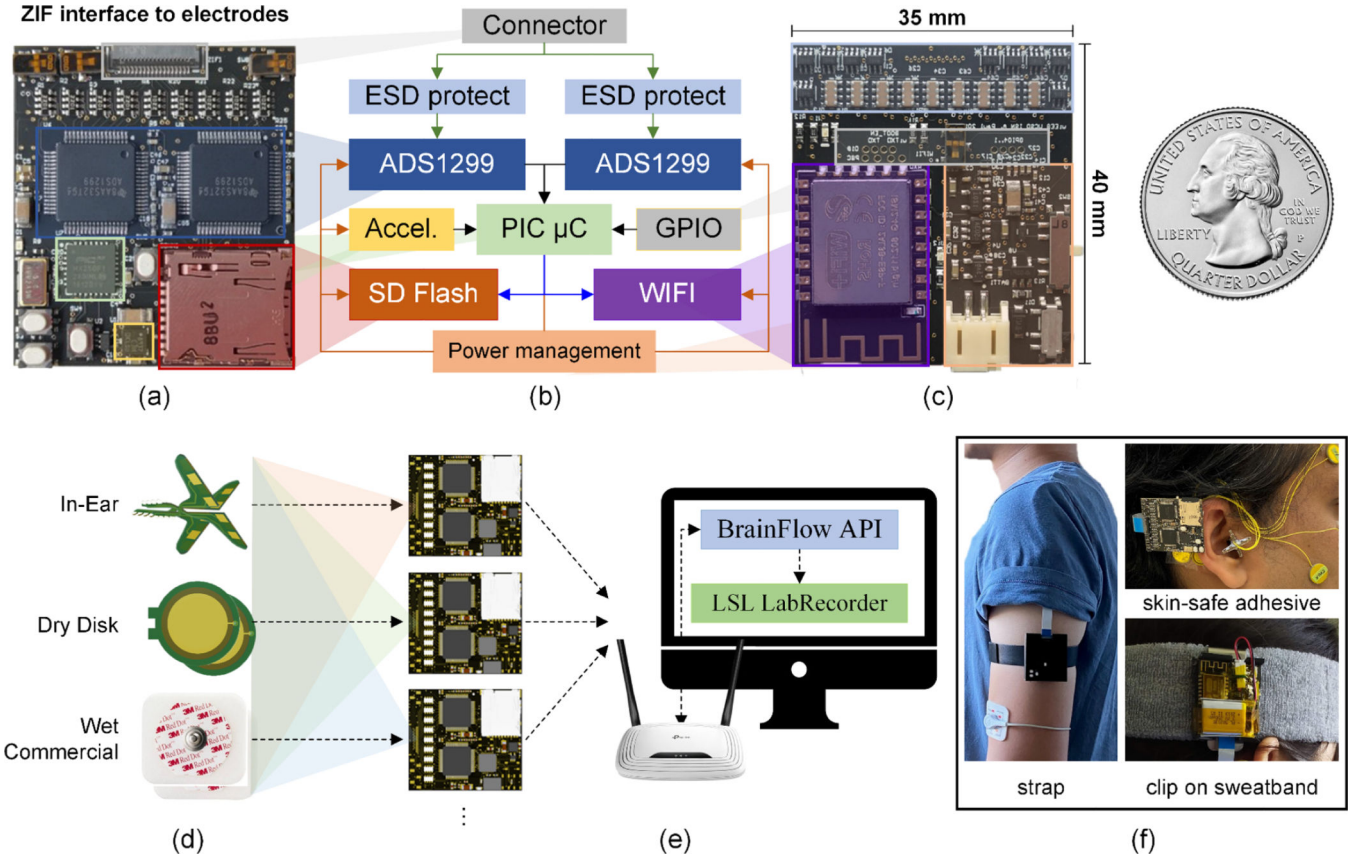

Fig. 6.

(a) Top side of weDAQ board. (b) System-level weDAQ block diagram. (c) Bottom side of weDAQ board. (d) Multiple electrode types shown to be compatible with weDAQ including Ag/AgCl in-ear, dry silver flat disk, and wet commercial. (e) Each weDAQ can interface with a mix of electrode types and multiple weDAQ devices can connect to a single access point for configuration control, triggering, and simultaneous streaming of data. (f) Depicts various wearable mounting solutions for the weDAQ.

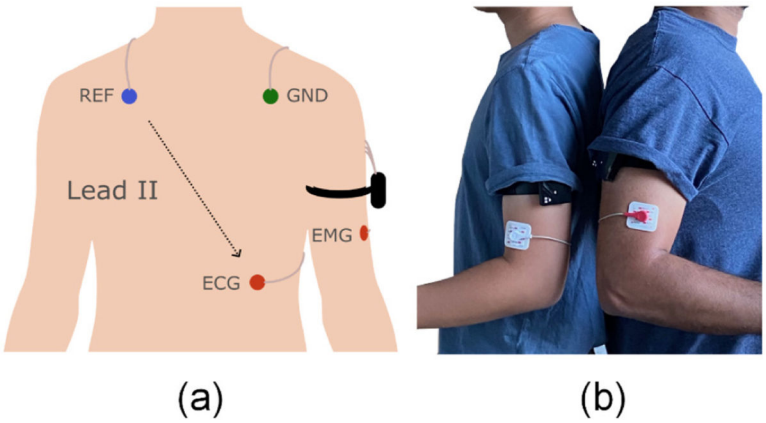

Fig. 7.

(a) Diagram of electrode placement for Lead-II ECG and Biceps EMG. (b) Photo taken during exercise experiment of 2 independent, untethered subjects being monitored by weDAQ devices on armbands as they are seated, standing, and lifting heavy objects.

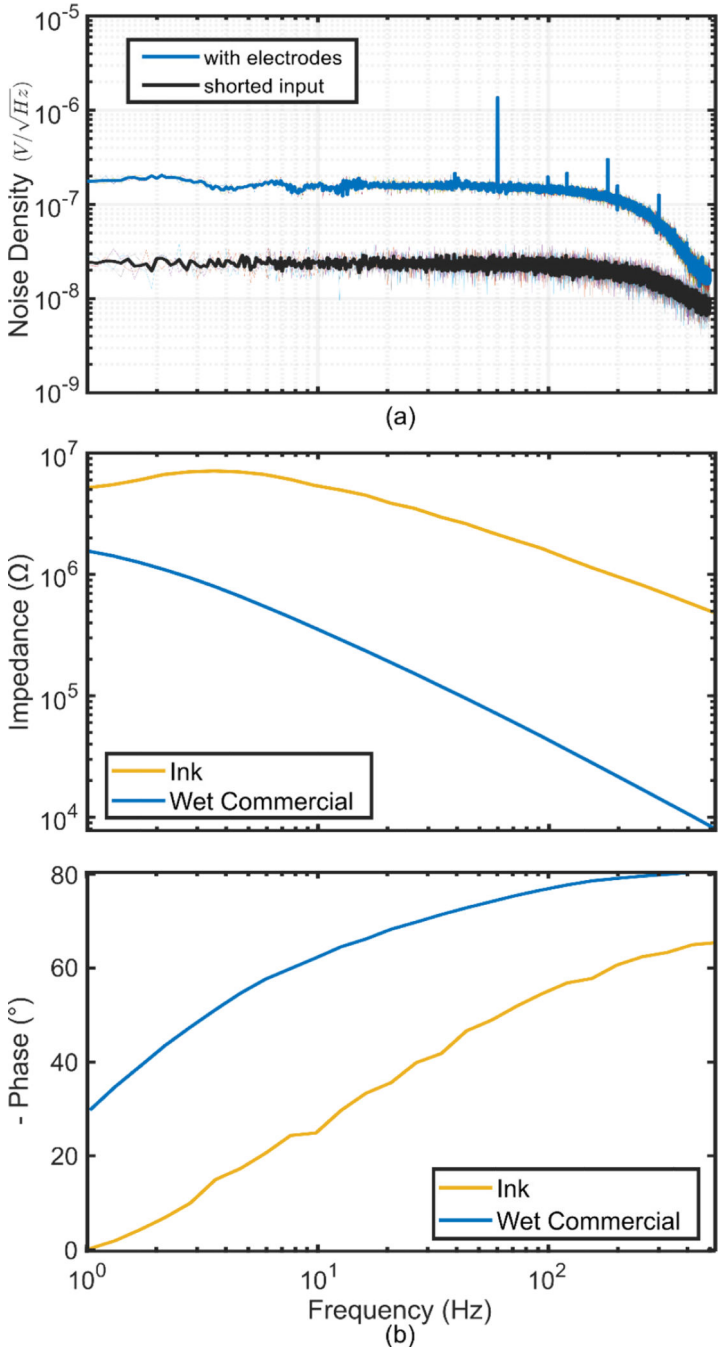

Fig. 8.

(a) Input-referred noise (IRN) spectra for the weDAQ measured with maximum device gain of 24 and 1 kHz sampling rate. (b) Impedance and phase profiles for Ag/AgCl ink applied to the PCB electrodes and commercial, gel Ag/AgCl electrodes.

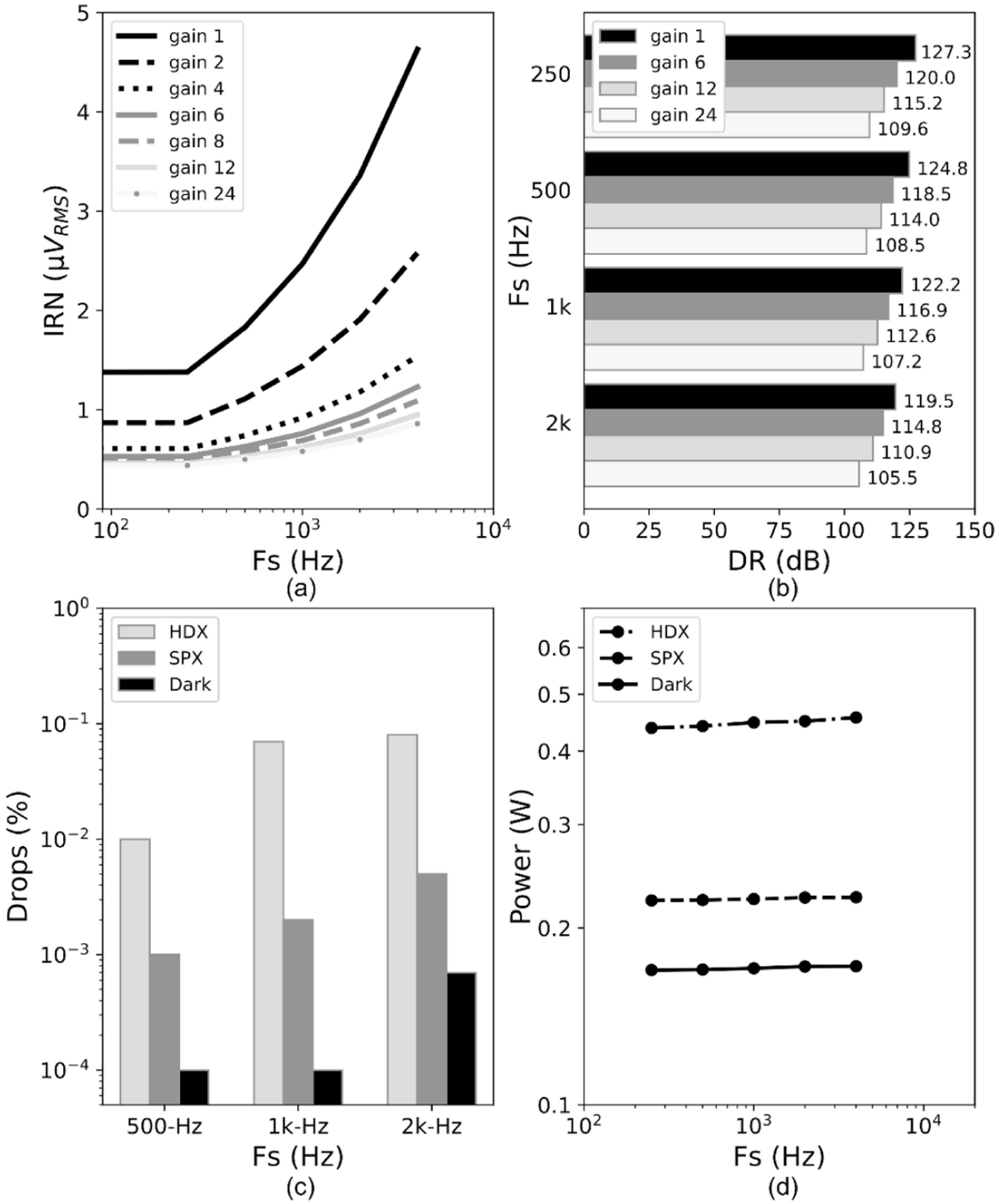

Fig. 9.

(a) Input-referred noise calculated from 0.01 Hz - 70 Hz across sampling frequencies (Fs) up to 4 kHz tested. (b) Dynamic range (DR) across gain settings. (c) Data drops, or corruption, observed for the main modes of operation. (d) Power consumption of the weDAQ across the tested sampling frequencies for the 3 main modes of operation.

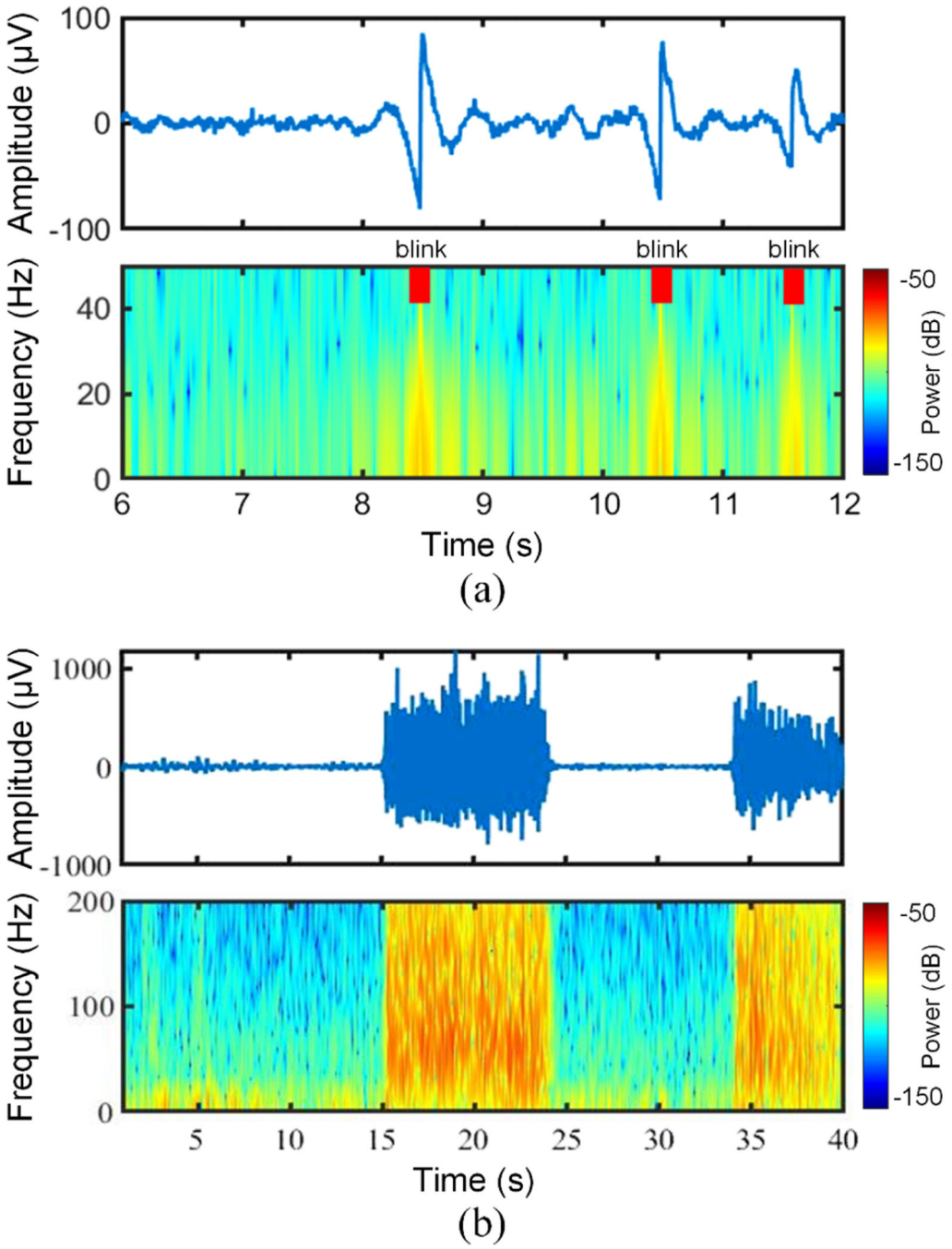

Fig. 10.

The spectrogram and time-series plot (a) of eye blinks and (b) EMG activity of the masseter muscle during jaw clenches, all recorded from in-ear channels.

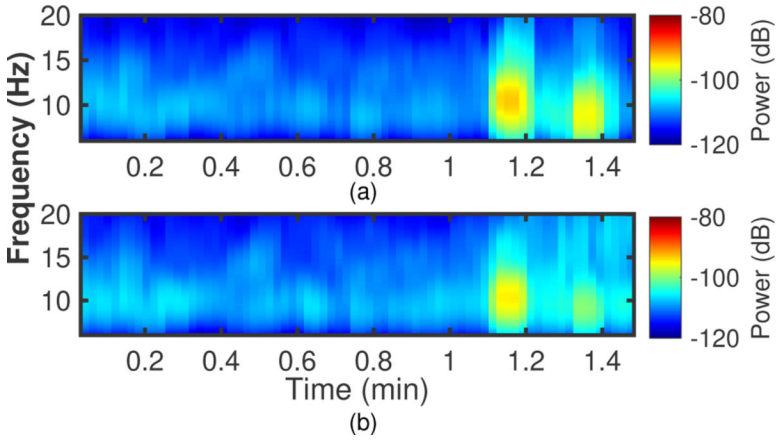

Fig. 11.

Spectrograms of EEG data captured during an eyes-closed alpha-power modulation task from (a) in-ear electrodes and (b) forehead electrodes. A rise in alpha-band power at around 10 Hz is observed for both the in-ear and forehead electrodes at approximately t = 1 min, corresponding with the time the subject closed their eyes.

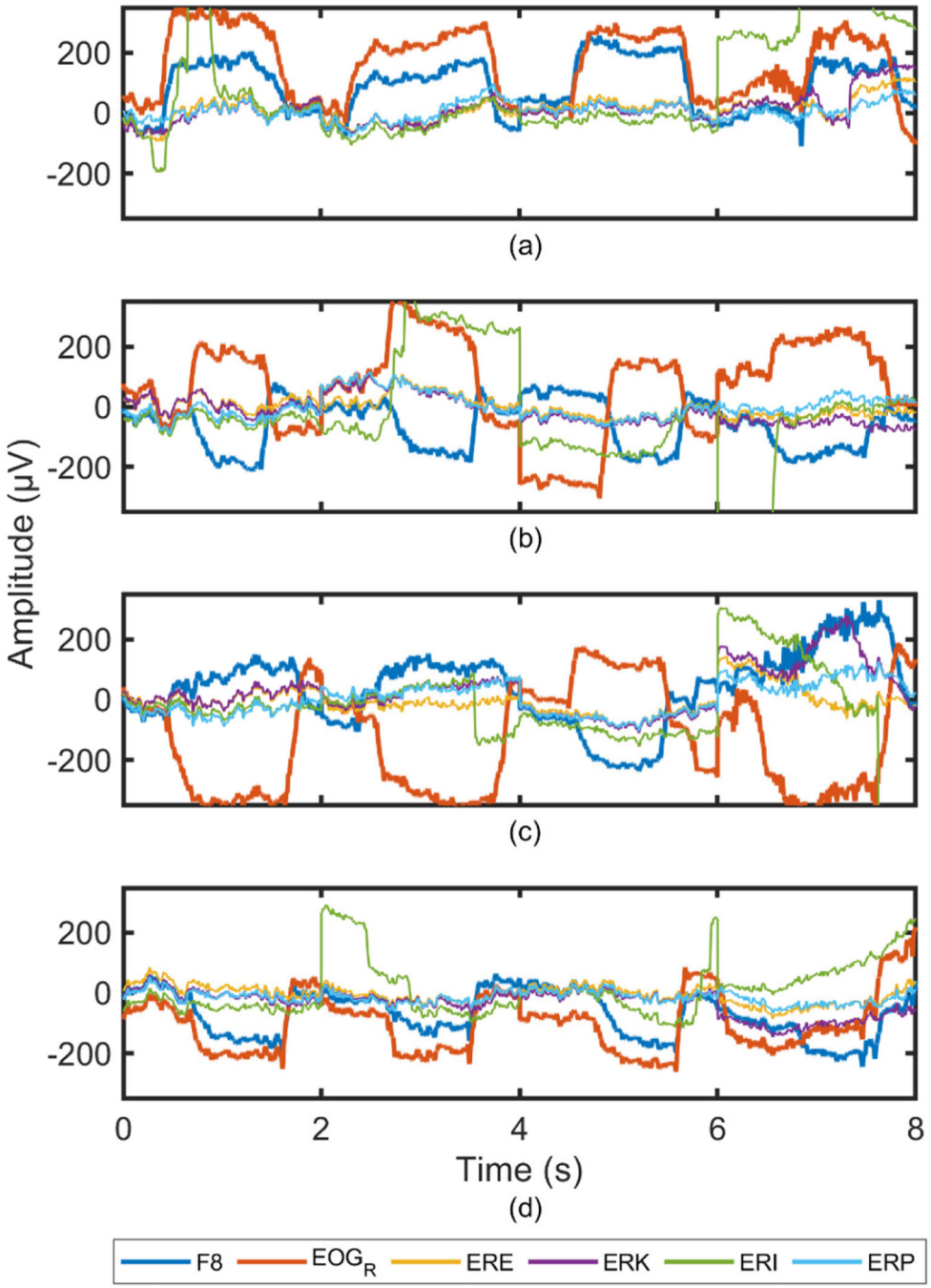

Fig. 12.

EOG activity captured during directional eye movements from center (a) leftward, (b) rightward, (c) upward, and (d) downward. Continuous EOG recording were made from 4 in-ear channels (sky blue, gold, purple, and green), 1 forehead EOG (blue), and 1 facial EOG (orange).

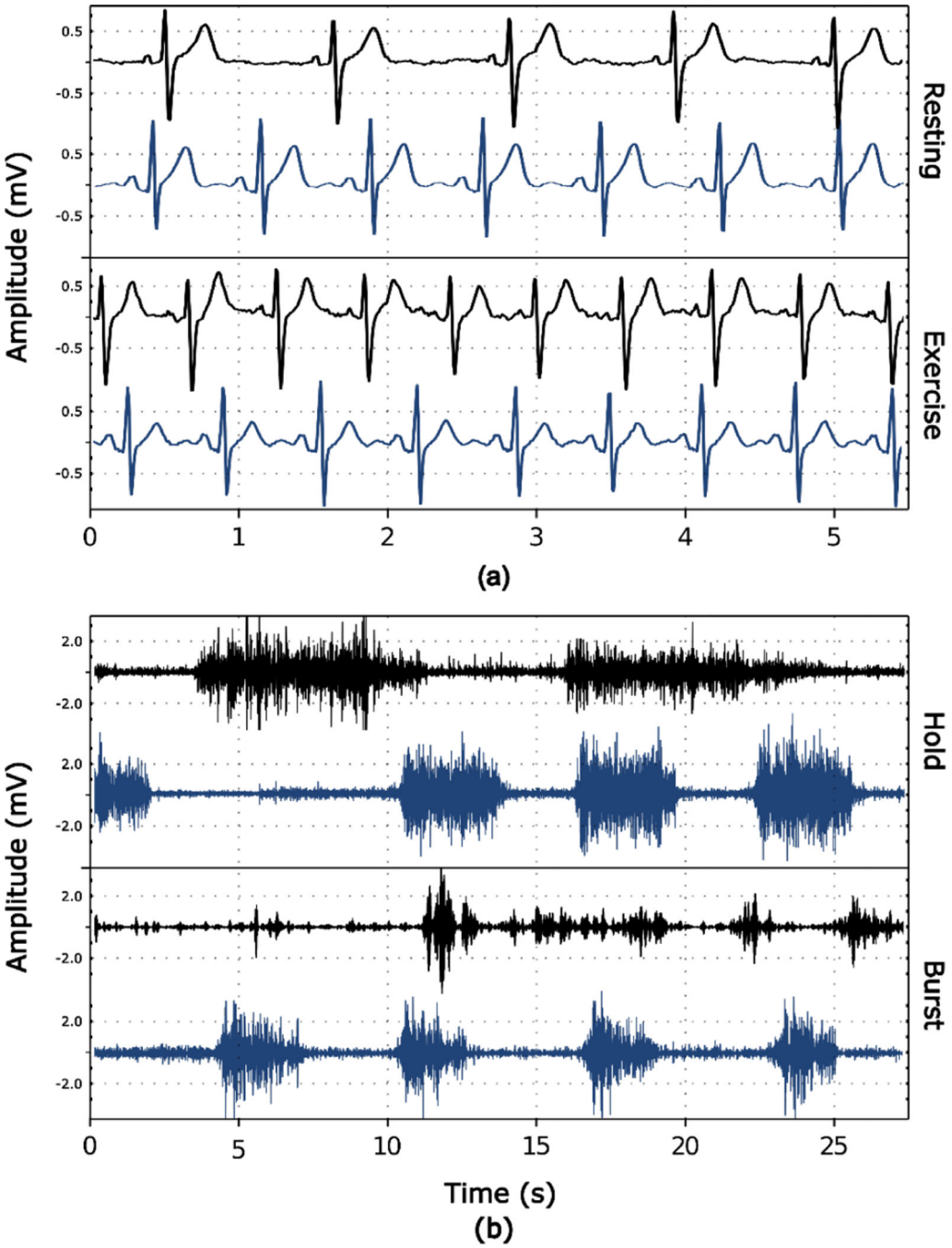

Fig. 13.

(a) ECG recordings were made of subject 1 (black) and subject 2 (blue) while seated and resting for baseline and following a brief period of high-intensity exercise. (b) Subjects were instructed to lift and hold heavy objects before placing them back down (Hold) and, separately, to quickly lift and release the objects (Burst).

TABLE I

WEDAQ Performance Benchmarks

Data Acquisition	
Sampling Rate	2000 Hz
Maximal Gain	27.6 dB
Noise (1000-Hz BW)	0.52 μV_{rms}
SNR	98.1 dB
CMRR	110.8 dB
Dynamic Range	105.5 dB
Power	0.171 W
Wireless	
Transmit Rate	54 Mbit/s
SD Write Speed	512 kbit/s
Energy Efficiency	5.5 nJ/bit
Reliability	< 0.005% drop

TABLE II

COMPARISON WITH ELECTROPHYSIOLOGY RECORDING SYSTEMS

	[15]	[22]	[21]	[43]	[16]†	[44]	[14]	This work
Channels	32	64	2	16	8	8	-	16
Sampling Rate	1000 Hz	1000 Hz	1000 Hz	-	250 Hz	500 Hz	1000 Hz	2000 Hz
Input Range	4.5 V_{pp}	0.1 V_{pp}	0.8 V_{pp}	0.9 V_{pp}	-	-	0.3 V_{pp}	4.5 V_{pp}
Bandwidth	100 Hz	1–500 Hz	0.5–100 Hz	0.5–100 Hz	100 Hz*	-	350 Hz	1000 Hz
IRN	1 μVrms	1.6 μV_{rms}	0.4 μV_{rms}	0.27 μV_{rms}	-	1 μV_{rms}*	<1 μV_{rms}*	0.52 μV_{rms}
IRN Density	100 $nV/\sqrt{Hz}$	70 $nV/\sqrt{Hz}$	57 $nV/\sqrt{Hz}$*	26 $nV/\sqrt{Hz}$	-	-	-	23 $nV/\sqrt{Hz}$
ADC Bit Resolution	24 bits	15 bits	11 bits	10 bits	24 bits	24 bits	24 bits	24 bits
Wireless	WiFi	Bluetooth	BCC‡	BCC‡	Bluetooth	WiFi	Bluetooth	WiFi
Power	-	46 mW	12.3 mW	16.1 mW	-	-	-	228.1 mW
Energy / Sample	-	1.4 μJ	61.8 μJ	10.1 μJ	-	-	-	7.1 μJ
Ref Channel MUX	Yes	-	No	No	Yes	-	-	Yes
Grounding	Active	Passive	Passive	None	Active	None	-	Active
Impedance Scanning	Yes	Yes	No	No	Yes	Yes	Yes	Yes

Values for each system presented in this table represent the configurations and metrics demonstrated in the corresponding references. It may be possible these systems have different performance metrics under different configurations but the values from the referenced works are taken as-is.

*Estimated value.

†Reference used the OpenBCI Cyton board [7].

‡Body-coupled communication (BCC) is shown in the references requiring a wired connection to the body.

TABLE III

COMPARISON WITH STATE-OF-THE-ART EAR EEG SYSTEMS

	[15]	[22]	[21]	[20]	[16]	[51]*	[14]	This work
Electrode Count	17	6	4	-	-	10	6	16†
Electrode Material	Ag/AgCl	Ag	-	Ag-Fabric	Ag paint	Ag/AgCl	IrO_2	Ag/AgCl
Electrode Contact	Dry	Dry	Dry	Wet	-	Dry	Dry	Dry
Reference	In-Ear	In-Ear	In-Ear	Behind Ear	External	External	In-Ear	In-Ear
Electrode Area	3.15 mm^2	60 mm^2	-	40 mm^2	-	-	9.6 mm^2	4.40 mm^2
Impedance 50Hz	20.42 $k\Omega cm^2$	226.44 $k\Omega cm^2$	-	-	-	10 $k\Omega$‡	1.1 $k\Omega cm^2$	52.78 $k\Omega cm^2$
Earpiece Style	Custom	Generic	Custom	Generic	Custom	Generic	Custom	Generic
Scalable	No	Yes	No	No	No	Yes	No	Yes
Sound Occluding	Yes	No	Yes	Yes	Yes	No	No	No

*This device is worn around the ear, not in-ear.

†Earpiece provides silver-plated pads for up to 16 electrodes.

‡Impedance is listed in reference without area of electrodes.